JOURNAL OF PROPULSION AND POWER
Vol. 27, No. 4, July–August 2011

Automated Design Optimization of a Three-Dimensional Subsonic Diffuser

Aniket Aranake*
Rutgers University, Piscataway, New Jersey 08854
Jin Gyu Lee
Agency for Defense Development, Daejeon 305-600, Republic of Korea
Doyle Knight*
Rutgers University, Piscataway, New Jersey 08854
and
Russell M. Cummings,† John Cox,† Micah Paul,† and Aaron R. Byerley†
U. S. Air Force Academy, USAF Academy, Colorado 80840

DOI: 10.2514/1.50522

An automated computational design optimization of a doubly offset (serpentine) subsonic diffuser is performed to assess the validity of a simple design principle for reducing flowfield distortion at the outlet. The design principle specifies that the flow be overexpanded within the bend, i.e., that the cross-sectional area in the bend exceed the cross-sectional area at the outlet. A baseline diffuser is defined as a monotonically increasing circular cross section following the specified doubly offset centerline. The design optimization uses a circular inlet and outlet that are identical to the baseline design, but permits a smooth blending of the cross section from circular to elliptical at the midpoint of the bend and returning to circular at the outlet while following the specified doubly offset centerline of the baseline design. The design variables of this study are the semimajor and semiminor axes of the ellipse at the midpoint. A commercial CAD program is used to loft the cross section smoothly from inlet to outlet. Turbulence is incorporated using a two-equation turbulence model. The automated computational design indicates that a substantial reduction in distortion is achieved by overexpanding the flow within the bend. Experimental evaluation of the baseline and optimal designs confirm an approximate 50% reduction in distortion coefficient for the optimal design compared with the baseline configuration, although the absolute values of the computed and experimental distortion coefficients differ.

I. Introduction

TYPICAL air-breathing jet engines use a subsonic diffuser to decelerate air entering the compressor. In many cases these diffusers have serpentine (S-shaped) geometries, which are made necessary by the location of an aircraft's inlets relative to its engine and also to minimize an aircraft's radar signature [1]. The aerodynamic performance of subsonic serpentine diffusers is principally determined by two parameters defined at the outlet of the diffuser, namely, 1) the distortion of the flow (described in Sec. II), and 2) the area-averaged total pressure recovery factor. Flow distortion in a serpentine diffuser is a direct consequence of the crossflow pressure gradients (due to the curvature of the diffuser centerline) that cause the formation of secondary flows. These secondary flows result in a nonaxisymmetric total pressure distribution at the compressor face, which can produce rotating stall in the compressor and also result in high-cycle fatigue of the compressor blades [2–5]. Specific design requirements for distortion have been established (see, for example, [3,6,7]).

The performance characteristics of curved subsonic diffusers has long been a topic of interest. As early as 1943, Weske [8] performed a series of experiments investigating the total pressure loss and velocity distributions of ducts with compound elbows. He concluded that the radius ratio (the radius of curvature of the centerline divided by the diameter of the duct) is the most significant variable contributing to the total pressure loss in a bend. Henry [9] developed empirical correlations for total pressure losses in subsonic diffusers of various shapes. Guo and Seddon [10–12] performed a series of experiments for S-shaped ducts with both horizontal and vertical offset to quantify the extent and influence of secondary flows. Additional experimental results along with qualitative analysis comparing diffuser design parameters to total pressure distortion are summarized in Seddon and Goldsmith [3] and Goldsmith and Seddon [13].

Computational studies have examined both the accuracy of numerical simulation of subsonic diffuser flows and their complex three-dimensional structure, with significant attention to the effect of the choice of turbulence models. Overall, studies have demonstrated reasonable agreement between computation and experiment. Harloff et al. [14] calculated a subsonic S-duct using the k-ϵ turbulence model [15] with modifications by Speziale et al. [16] and achieved good agreement with experiment. Abrahamsen et al. [17] computed a subsonic S-duct using the k-ϵ turbulence model with modifications by Chien [18] and achieved good agreement with surface pressure distributions along the length of the duct. Zhang et al. [19] achieved good agreement with the experimental measurements of Wellborn et al. [20] for distortion coefficients in an S-shaped diffuser using the Baldwin–Lomax [21] algebraic turbulence model. An investigation performed by Smith et al. [22] found good agreement between experimental data and results computed also using the Baldwin–Lomax [21] turbulence model. This same study also predicted that a two-equation model would provide even better results in S-shaped ducts. Lee and Kim [23] performed a sensitivity study of S-shaped diffusers using different turbulence models. They conclude that the shear stress transport (SST) k-ω two-equation model, based upon the work by Kolmogorov [24] and Saffman [25], was best suited for this problem.

Various optimizations have been performed to improve the performance characteristics of subsonic diffusers by reducing distortion

Received 26 April 2010; revision received 13 January 2011; accepted for publication 13 January 2011.

*Department of Mechanical and Aerospace Engineering, 98 Brett Rd.
†Department of Aeronautics.

Table 1 Baseline diffuser control points and cross-sectional area

Control point	x, cm	y, cm	z, cm	D, cm	Area, cm^2
0	−30.00	0.00	0.00	10	78.54
1	−25.00	0.00	0.00	10	78.54
2	−20.00	0.00	0.00	10	78.54
3	−10.00	0.00	0.00	10	78.54
4	0.00	0.00	0.00	10	78.54
5	8.33	5.28125	0.00	10.5625	87.62
6	16.67	10.5625	0.00	11.125	97.21
7	20.835	10.5625	0.00	11.125	97.21
8	25.00	10.5625	0.00	11.125	97.21
9	33.30	10.5625	5.28125	11.6875	107.28
10	41.67	10.5625	10.5625	12.25	117.86
11	50.00	10.5625	10.5625	12.25	117.86
12	60.00	10.5625	10.5625	12.25	117.86
13	65.00	10.5625	10.5625	12.25	117.86
14	70.00	10.5625	10.5625	12.25	117.86

while maintaining (or increasing) total pressure recovery. Two principal methods have been employed, namely, 1) boundary-layer control devices (e.g., vortex generators on the diffuser sidewalls), and 2) diffuser cross-sectional shape modification.

Several examples of vortex generators applied to subsonic diffusers may be cited. Kaldschmidt et al. [26] investigated the effect of vortex generators on an S-duct diffuser for the Boeing 727 aircraft. Anderson [27] evaluated a variety of vortex generator configurations for a subsonic S-duct and achieved an 80% reduction in distortion. Jirásek [28] evaluated experimentally the effect of vortex generator geometry and placement on the flowfield distortion and total pressure recovery at the outlet of two serpentine inlets. It should be noted, however, that vortex generators have a large number of design parameters (see Table 1 in Anderson [27] and Table 1 in Jirásek [28]), thus complicating the search for an optimal design.

Several examples of the diffuser cross-sectional shape modification can be cited. Mayer et al. [29] performed a series of computations for serpentine subsonic diffusers and concluded that the curvature of the duct centerline had the strongest influence on the total pressure recovery at the outlet. Cholaseuk et al. [30] performed an automated design optimization of two-dimensional and axisymmetric diffusers for laminar flow Reynolds numbers. Lefantzi and Knight [31] used an automated technique to improve the performance of an S-shaped diffuser by introducing a bump midway through the diffuser which generated streamwise vorticity, thereby enhancing mixing and reducing distortion. Lim and Choi [32] optimized a two-dimensional subsonic diffuser using an adjoint-based gradient algorithm to achieve virtually zero wall shear stress. Saha et al. [33] explored the effect of varying the cross-sectional geometry at the inlet of the diffuser. Of the shapes they have considered, they found that a semicircular inlet produces the least amount of distortion, followed by an elliptical inlet. Lee and Kim [23] used an adjoint method to improve the design of a baseline S-shaped diffuser circular cross section. The result of this technique warped the initially circular cross section into oblong shapes and by doing so improved the pressure recovery and distortion index.

The objective of the present study is to determine a simple design principle for the cross-sectional shape of the serpentine diffuser as a function of position that results in reduced distortion in a serpentine subsonic diffuser while maintaining high total pressure recovery. A doubly offset serpentine geometry with monotonically increasing circular cross section is chosen as the baseline design. A monotonically increasing cross-sectional area is, of course, the standard approach to subsonic diffuser design [3,13]. An automated design optimization of the shape of the diffuser is performed allowing the cross-sectional shape at the midpoint of the bends to be elliptical with arbitrary values of major and minor axes, i.e., permitting the cross-sectional area at the midpoint to have an arbitrary cross-sectional area and noncircular shape.

Previous computational optimization studies (e.g., [23,30,31,33]) have presented ad hoc shape changes which reduced flow distortion at the outlet; however, these studies lacked a definitive conclusion regarding any design principle(s) for reducing distortion in an S-shaped diffuser compared with the conventional circular cross-sectional baseline design. We address this issue in Sec. IV.D.

II. Problem Statement

A. Baseline Diffuser

The baseline diffuser used in this optimization is shown in Fig. 1. The endpoints of the centerline are chosen such that the diffuser will be doubly offset, i.e., the endpoints are chosen so that the airflow translates in both the y and z directions from the inlet to the outlet. The baseline design is a straightforward interpolation between these two end points. The centerline of this diffuser is defined by a spline through a set of control points that are given in Table 1. The size of the diffuser was selected to fit in the test section of the wind tunnel at the U.S. Air Force Academy, which is 3 ft (91.5 cm) in length. The diffuser has a circular cross section throughout, increasing monotonically in area from 78.5 cm^2 (5 cm radius) at the inlet to 117.9 cm^2 (6.125 cm radius) at the outlet to give the desired outlet ratio of $A_{\text{outlet}}/A_{\text{inlet}} = 1.5$.

B. Design Objectives

The present study is a Pareto optimization with two design objectives. The first is to maximize the total pressure at the outlet of the diffuser since it translates directly into the amount of work that can be extracted from the flow. The total pressure recovery factor is a ratio of total pressures given by

$$\text{PR} = \frac{\bar{p}_{o,\text{outlet}}}{\bar{p}_{o,\text{inlet}}} \tag{1}$$

where the mean total pressures at the inlet and outlet are defined as

$$\bar{p}_0 = \frac{\int_0^{2\pi}\int_0^R p_0(r,\theta) r \,\mathrm{d}r \,\mathrm{d}\theta}{\int_0^{2\pi}\int_0^R r \,\mathrm{d}r \,\mathrm{d}\theta} \tag{2}$$

For an isentropic diffuser, the total pressure remains constant and the pressure recovery is one. In practice, subsonic diffusers are nearly isentropic, and typical pressure recovery factors are greater than 0.95.

The second design objective is to minimize the distortion at the diffuser outlet. The distortion coefficient is defined as

$$\text{DC}(\psi) = \max_{0\le\phi\le 2\pi} \frac{[\bar{p}_0 - \bar{p}_0(\phi,\psi)]}{\bar{q}} \tag{3}$$

where $\bar{q}$ is the mean dynamic pressure with $q = \frac{1}{2}\rho V^2$, where ρ is the density and V is the magnitude of the velocity, and $\bar{p}_0$ is the mean total pressure. All values are evaluated at the diffuser outlet. The distortion coefficient is a measure of the nonaxisymmetry of the

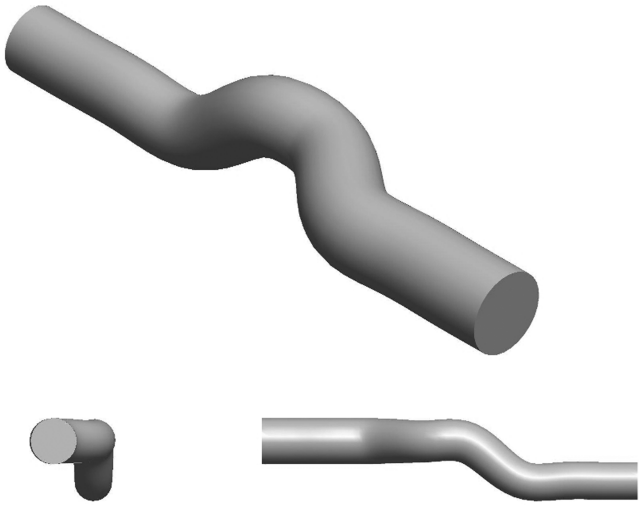

Fig. 1 Baseline diffuser.

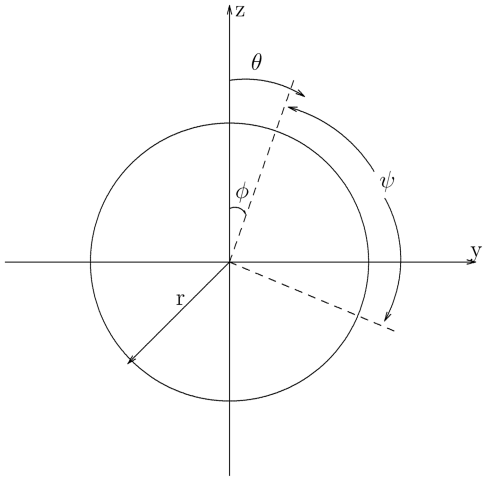

Fig. 2 Sample of pie-slice used to calculate distortion coefficient.

outlet flow. The angle ϕ is the starting angle of a pie-shaped slice of angle ψ over which the total pressure is integrated. The terms of Eq. (3) are defined as follows:

$$\bar{p}_0(\phi,\psi) = \frac{\int_0^{\psi}\int_0^{R} p_0(r,\phi+\theta)r\,\mathrm{d}r\,\mathrm{d}\theta}{\int_0^{\psi}\int_0^{R} r\,\mathrm{d}r\,\mathrm{d}\theta} \tag{4}$$

$$\bar{q} = \frac{\int_0^{2\pi}\int_0^{R} qr\,\mathrm{d}r\,\mathrm{d}\theta}{\int_0^{2\pi}\int_0^{R} r\,\mathrm{d}r\,\mathrm{d}\theta} \tag{5}$$

The angles involved in the calculation of the distortion coefficient are shown in Fig. 2, with $\psi = 60°$ in Eq. (3). Similar coefficients have defined for different pie-slice angles ψ (DC(45), DC(90), etc). Previous studies show that results are similar for different values of ψ [19], so this study only considers DC(60).

C. Design Variables

For each iteration of the optimization, the diffuser cross section follows the shape pattern outlined in Table 2. A sample design is depicted in Fig. 3. The elliptical cross section at control point 7 is defined by the following equation:

$$\frac{y^2}{a^2} + \frac{z^2}{b^2} = 1 \tag{6}$$

where y and z are Cartesian coordinates (relative to the centerline of the diffuser) and a and b are the design variables. The values of a and b were limited to the range

$$4\text{ cm} \le a \quad \text{or} \quad b \le 7\text{ cm} \tag{7}$$

D. Flow Conditions

The flow conditions at the diffuser inlet are fixed for this study. The selected inlet Mach number is $M_\infty = 0.3$ and the inlet total pressure is $p_{t_\infty} = 0.8p_{\text{sealevel}}$ or $8.1 \cdot 10^4$ Pa. This is the standard day pressure at the location of the U.S. Air Force Academy, where the results of this study were experimentally verified. The total temperature, selected for the same elevation, is $T_{t\infty} = 276°\text{K}$. From these three conditions, the remaining flow parameters are derived as indicated in Table 3.

Table 2 Optimization design geometry rules

Position	Rule
$-30\text{ cm} \le x \le -20\text{ cm}$	Constant circular cross section, $d = 10.0$ cm
$-20\text{ cm} < x < 20.835\text{ cm}$	Circular cross section blending into ellipse
$x = 20.835$ cm	Elliptical cross section, described by optimization variables
$20.835\text{ cm} < x < 60\text{ cm}$	Elliptical cross section blending into circle
$60\text{ cm} \le x \le 70\text{ cm}$	Constant circular cross section, $d = 12.25$ cm

[a]$x = -30$ cm is the position of the diffuser inlet.

E. Summary of Problem Statement

The design optimization problem is as follows: determine the Pareto set of optimal designs to 1) maximize PR, and 2) minimize DC (60) at the outlet using as design variables the midpoint cross-section semi-axes a and b subject to Eq. (7) for the flow conditions indicated in Sec. II.D.

III. Methodology

A. Optimization Loop

This study performs an optimization using commercially available software programs. The optimizer used is the multi-objective genetic algorithm MOGA-II, which is included in the commercial software Esteco modeFRONTIER.[‡] Fig. 4 shows the software programs used in the optimization loop. Execution of these programs and the sharing of data between them is handled by modeFRONTIER.

PTC Pro/ENGINEER Wildfire 3.0[§] is used for solid modeling. The diffuser geometry is generated by first creating a fixed cubic spline through the centerline points specified in Table 1. A swept blend feature is then used to create a surface interpolating the cross-sectional geometries which are specified at each of these control points. For the case of the baseline diffuser, these cross sections are circles of a given diameter. For optimization designs, the cross sections are identical to the cross sections of the baseline at points 0 through 3, which represent the diffuser inlet, and 12 through 14, which represent the diffuser outlet. The cross section at point 7 is the ellipse of which the semimajor and semiminor axis are the optimization variables of this study. All intermediate cross-sectional geometries are determined by Pro/ENGINEER's internal interpolation technique, which blends the surface smoothly from the inlet to the outlet.

The geometry is exported from Pro/E in STEP format and passed on to the grid generator. Grid generation for this study is performed using Ansys Gambit.[¶] A boundary-layer mesh is attached to the wall of each diffuser design, and a hex cooper unstructured grid is generated for interior points. A wall function is not used, so the distance h between the wall and the first grid point is controlled manually. A value of $h = 1.0 \cdot 10^{-5}$ m was found to satisfy the condition that the max y^+ value is approximately 1.0, where y^+ is the dimensionless normal distance of the first grid point from the wall [34].

The flow solver Ansys Fluent[**] is used to solve the incompressible Navier–Stokes equations numerically with SIMPLE pressure-velocity coupling. Based on the results obtained by Lee and Kim [23], the SST k-ω model is selected. For inlet conditions, a turbulent intensity of 1% and a hydraulic diameter of 0.1 m are specified in addition to a uniform velocity. Second-order upwind schemes are used for discretization, and a successive underrelaxation scheme is used to iterate to the steady state solution.

Based on the results obtained from the flow solver, the MOGA-II algorithm selects the next design to evaluate. This process loops so that an optimal set of designs is obtained.

B. Grid Refinement

The appropriate grid resolution in an optimization loop balances computational time and accuracy. A higher grid resolution provides a more accurate result but at a substantial computational cost.

[‡]Additional data available online at http://www.esteco.com/ [accessed May 2008].

[§]Additional data available online at http://www.ptc.com/products/proengineer/ [accessed May 2008].

[¶]Additional data available online at http://www.ansys.com/ [accessed May 2008].

[**]Additional data available online at http://www.ansys.com/products/fluid-dynamics/fluent/ [accessed May 2008].

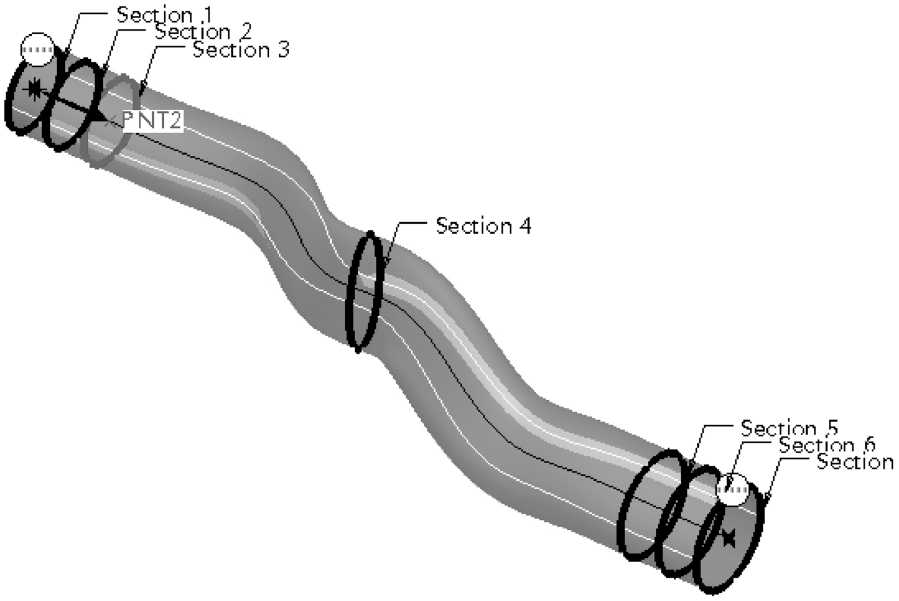

Fig. 3 Sample design diffuser.

Additionally, a certain minimum grid resolution is to reasonably capture a diffuser geometry and flow characteristics such as separation.

A grid refinement study was performed to test the effect of increasing the resolution in both the azimuthal direction and the streamwise directions. Grid resolution is enumerated by the dividing numbers, N_θ, which divides the geometry radially in the y-z plane, and N_x, which divides the geometry in the x-direction. The dependance of PR and DC(60) on each of these terms is shown in Fig. 5. It is seen in this figure grid convergence depends more on the dividing number N_x than on N_θ. With $N_x = 225$, the pressure recovery is converged to within 10^{-4}, which is the precision to which this parameter is calculated. The distortion coefficient at the same dividing number has also converged. Between successive calculations ($N_x = 200$ and $N_x = 225$), the DC(60) changes by at most 0.02. The numerical accuracy at this level is within 7%.

Table 3 Flow parameters

Parameter	Value
T_∞, deg K	271.1
U_∞, m/s	99.01
ρ_∞, kg/m^3	0.978
p_∞, kPa	76.1
Re_∞, m^{-1}	$5.7 \cdot 10^4$

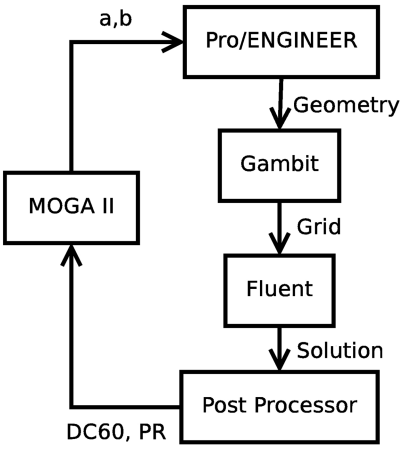

Fig. 4 Optimization loop in mode FRONTIER.

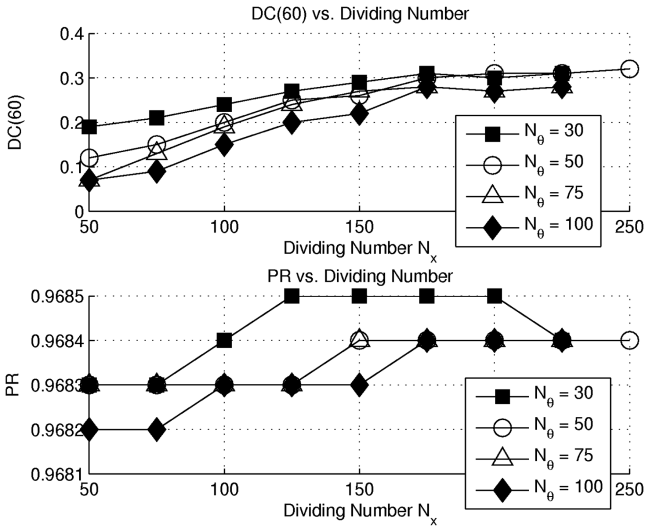

Fig. 5 Results of grid refinement study.

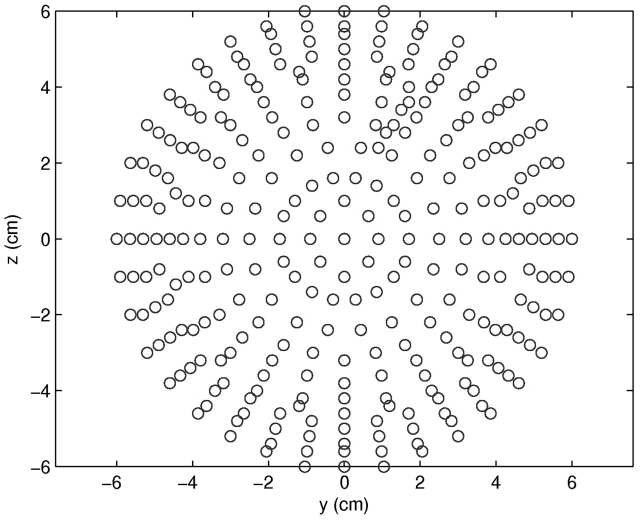

Fig. 6 Experimental measurement locations.

While fine grid resolution provides accurate results, the time required to solve fine grids can be prohibitive. This is especially problematic in an optimization which must run many simulations. For this reason, a coarse grid with $N_x = 125$ and $N_\theta = 60$ was used in the optimization loop. When the loop completed, select designs from the resultant Pareto set were recalculated using a fine grid with $N_x = 225$ and $N_\theta = 150$. The approximate time required to compute a solution using the coarse grid is 2 h, while the required time for a fine grid solution is 12 h. These times are for simulations each running on three 1.8 GHz AMD Opteron processors.

C. Experimental Setup

The results of the computational fluid dynamics (CFD) calculations were verified experimentally at the U.S. Air Force Academy in Colorado Springs, Colorado. Using a combination of rapid prototyping and traditional machining techniques, models of both the baseline and an optimized diffuser (Design 44 as discussed in Sec. IV.A) were generated. The flow characteristics of these models was tested in the U.S. Air Force Academy Subsonic Wind Tunnel, which is capable of speeds of up to $M = 0.6$.

A 5-hole probe connected to a Pressure Systems 8400 was used to take readings of total pressure at the outlet plane. This instrument was mounted on a 2 °-of-freedom traverse, which moved the probe to a given y-z coordinate. To capture the behavior of the outlet airflow, a total of 290 probe locations was selected, and a total pressure measurement was taken at each of these locations. The pattern of locations selected is shown in Fig. 6. Following a time delay which allowed the flow to stabilize, data was sampled from the 5-hole probe at 25 Hz for 4 s at each of these probe location. The resulting 100 data values for each probe location were averaged to establish the total pressure at that location. This setup provides measurements that are accurate to within 0.06%.

Throughout the experiment, an MKS Instruments transducer built into the wind tunnel was used to measure the static and total pressures inside the tunnel. Ambient pressure was measured using a Setra digital pressure gage. These pressure measurements, as well as measurements of temperature inside the wind tunnel and ambient temperature, were sampled at a rate of 2 Hz. Static pressure measurements are accurate to within 0.15% and total pressure measurements are accurate to within 0.05% [35,36].

IV. Results

A. Pareto Set

In total, the MOGA-II algorithm explored 94 diffuser designs. The relevant portion of the design space is shown in Fig. 7. Each of the points in this plot is designated by a design number. This plot shows

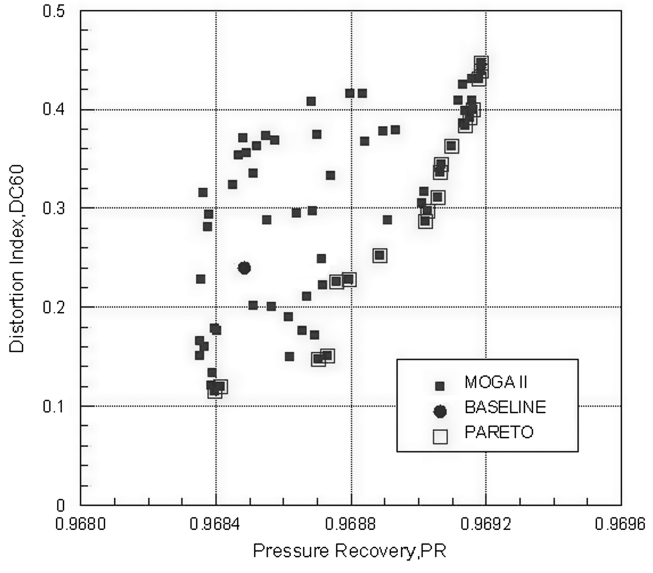

Fig. 7 Design space explored by MOGA-II.

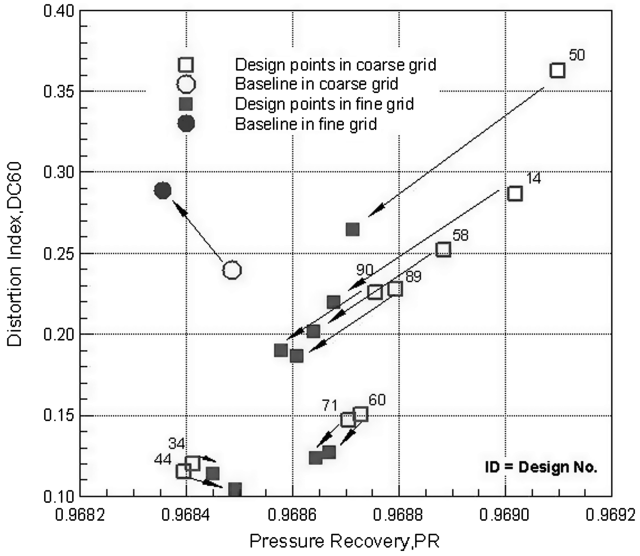

Fig. 8 Result of refining mesh on Pareto optimal designs.

the distortion coefficient plotted against the total pressure recovery coefficient and highlights the Pareto set. Nine designs from the Pareto set were selected for a grid refinement study. The solution for these nine designs was recalculated using the fine mesh previously described. The refined results shifted the locations of these points in the design space as shown in Fig. 8. A total of five designs remain in the Pareto set and are listed in Table 4 together with the baseline design. Several key results are evident:

1) The total pressure recovery coefficient PR is virtually the same for all designs in the Pareto set and essentially the same as the baseline PR. Therefore, the distinguishing design objective is the distortion coefficient DC(60).

2) There is an *inverse* relationship between the area ratio, defined as the ratio of the cross-sectional area at the midpoint to the outlet cross-sectional area, and the distortion coefficient for the Pareto set. In particular, the lowest distortion coefficient is achieved for the largest area ratio. However, the largest area ratio (corresponding to design 44 with $a = 6.69$ cm and $b = 6.63$ cm) is not the largest allowable area ratio (which corresponds to $a = b = 7$ cm from Eq. (7)).

3) The designs with the greatest improvement in distortion coefficient (i.e., design nos. 44, 71 and 60, each of which reduced the distortion coefficient by more than 50% compared with the baseline) *overexpand* the flow at the midpoint (i.e., the area ratio exceeds unity). Since the control points were fixed for all designs (Table 1), therefore the lowest distortion coefficient is achieved for the largest rate of increase of the overexpansion in the midsection.

4) There is an *inverse* relationship between the eccentricity ϵ of the cross-sectional area at the midsection defined by

$$\epsilon = \sqrt{1 - \left(\frac{b}{a}\right)^2}$$

and the distortion index for the Pareto set. An eccentricity $\epsilon = 0$ corresponds to a circle, and thus it is evident that the lowest distortion coefficient (design 44) is achieved for a *nearly circular, overexpanded cross section* at the midpoint.

B. Comparison of Computation and Experiment

The experimental geometry is design 44. To have a proper comparison between computational and experimental results, the computational data is first interpolated to the pressure probe locations. This is done using a MATLAB script which finds the pressure at each probe location by performing a planar interpolation of the nearest three computational grid nodes. The script then finds the distortion coefficient by performing a numerical integral on both

Table 4 Computed baseline and optimal designs

Design	a, cm	b, cm	PR	DC(60)	Area ratio	ϵ
Baseline	5.56	5.56	0.9684	0.2833	0.8248	0.0
Design 44	6.69	6.63	0.9685	0.1038	1.1823	0.1336
Design 71	6.92	5.58	0.9686	0.1234	1.0293	0.5914
Design 60	7.00	5.53	0.9687	0.1269	1.0318	0.6131
Design 14	6.71	4.71	0.9687	0.2192	0.8424	0.7122
Design 50	7.00	4.22	0.9687	0.2645	0.7874	0.7978

[a]1) PR and DC(60) computed using *all* cells in computational grid. 2) Area ratio is the ratio of the area at the midpoint to the outlet area. The outlet area is 117.86 cm^2 for all cases. 3) The eccentricity ϵ is defined as

$$\epsilon = \sqrt{1 - \left(\frac{b}{a}\right)^2}$$

the experimental and interpolated computational data sets. For this comparison, the distortion coefficient redefined as follows:

$$\mathrm{DC}(60)_\infty = \max_{0\le\phi\le 2\pi} \frac{[\bar{p}_0 - \bar{p}_0(\phi, 60^\circ)]}{\frac{1}{2}\rho_\infty U_\infty^2} \tag{8}$$

A minor difference between this definition and Eq. (3) is that the normalization in this case is done with respect to the entrance conditions rather than local or outlet conditions. This was done because local outlet values of density and velocity are not available in the experimental case.

The computed and experimental total pressure recovery coefficient PR and distortion coefficient $\mathrm{DC}(60)_\infty$ are shown in Table 5. Although the computed and experimental absolute values of $\mathrm{DC}(60)_\infty$ are significantly different for each configuration, the percentage reduction in $\mathrm{DC}(60)_\infty$ is very similar (50% for the experiment and 56% for the simulation as indicated in Table 6). Thus, the optimization captures the correct trend in redesigning the diffuser to reduce the distortion at the outlet. The difference in absolute values of $\mathrm{DC}(60)_\infty$ may be attributed to two factors. First, the distortion coefficient is sensitive to the placement and number of measurement points at the outlet. This is apparent from the variation in the computed distortion coefficient between Table 4 (which calculated DC(60) using *all* computational grid cells) and Table 5 (which calculated $\mathrm{DC}(60)_\infty$ using computed results interpolated to the experimental measurement locations in Fig. 6). As indicated in Sec. IV.C, the total pressure contours at the outlet display large gradients over a portion of the outlet, and consequently a small difference between computation and experiment can account for a significant difference in $\mathrm{DC}(60)_\infty$. Second, the computed total pressure profile at the outlet is undoubtedly dependent on the computed structure of the separated flow model. Although previous studies have considered the SST k-ω model to be the best choice among two-equation turbulence models for diffuser flows [23], there is nonetheless an influence of the turbulence model on the value for $\mathrm{DC}(60)_\infty$. Nevertheless, the important result is the close agreement between the predicted percentage reduction in $\mathrm{DC}(60)_\infty$ between computation and experiment.

The total pressure recovery coefficient PR is insensitive to the changes in the geometry between the baseline and optimal designs.

Table 5 Comparison of computation and experiment

Case	$\mathrm{DC}(60)_\infty$	PR
Baseline, experimental	0.0762	0.9829
Optimized, experimental	0.0383	0.9855
Baseline, CFD	0.187	0.9685
Optimized, CFD	0.0821	0.9685

[a]$\mathrm{DC}(60)_\infty$ and PR calculated using only experimental measurement locations.

Table 6 Improvement from baseline to optimized

Method	Distortion reduction
Experiment	50%
Computation	56%

[a]Results from Table 5.

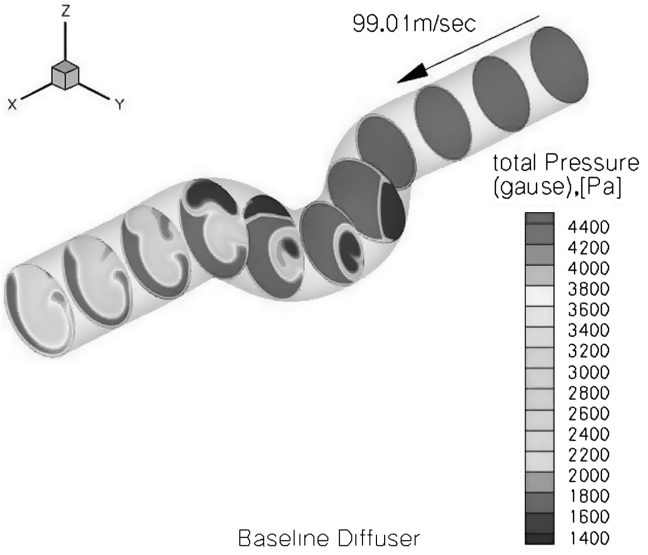

Fig. 9 Total pressure contours: baseline diffuser.

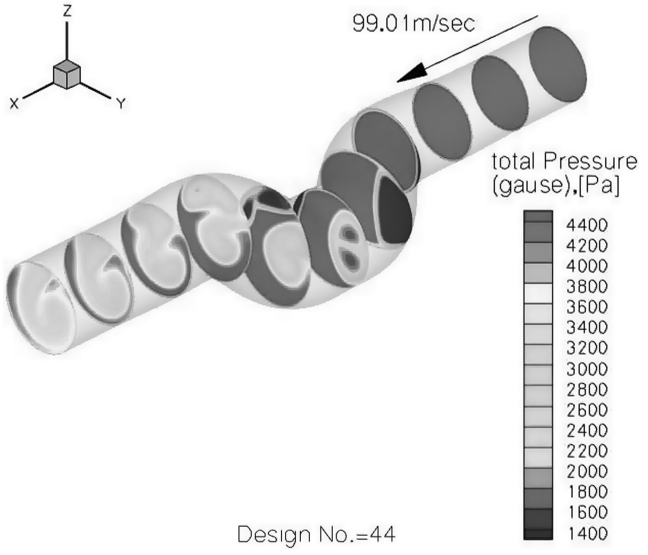

Fig. 10 Total pressure contours: optimized diffuser.

The experimental PR varies by 0.2%. The computed PR does not change.

C. Discussion

The reduction in the computed distortion coefficient between the baseline and nesign 44 (hereinafter denoted the "optimized case") is observed visually as a reduction in the nonaxisymmetry of the total pressure at the outlet. Figure 9 shows the computed total pressure contours at selected streamwise locations from inlet to outlet for the baseline design. The large azimuthal variation in total pressure near the wall at the outlet leads to a high distortion coefficient. In the case of the computed optimized diffuser, shown in Fig. 10, the variation in total pressure at the outlet is visibly reduced, thus leading to a lower distortion coefficient.

The physical mechanism for the reduction in distortion is enhanced three-dimensional mixing of the flow due to the overexpansion in the midpoint. This is evident in the comparison of the mean streamlines for the baseline (Fig. 11) and optimized (Fig. 12) diffusers. In each figure, a set of streamlines originate at the inlet at a radius of 4 cm (i.e., 80% of the inlet radius) with equal azimuthal spacing of 45°. Several of the streamlines in the optimized diffuser display far more circulatory (azimuthal) motion than in the baseline diffuser, thereby implying a greater azimuthal mixing of the flow and reduction in nonaxisymmetry.

Our understanding of the physical mechanism for the enhanced mixing is limited due to the lack of a simple three-dimensional model for such a phenomenon in subsonic flow. Nevetheless, three major physical factors can be identified [37]. First, the curvature of the centerline induces a cross-flow pressure gradient leading to the formation of a swirling azimuthal flow which is enhanced in the boundary layer where the fluid momentum is less than in the inviscid core. Second, the increase in cross-sectional area retards the flow, and at a sufficient magnitude can create an adverse streamwise pressure gradient sufficient to cause boundary-layer separation [37]. Both effects are present in the baseline and optimized diffusers; however, the second effect is more pronounced for the optimized diffuser due to the overexpansion at the midpoint (i.e., the adverse pressure gradient is larger for the optimized diffuser). Figure 13 compares the area ratio (see Sec. IV.A) vs arclength along the diffuser centerline s, normalized by the inflow diameter D, for the baseline and optimized (design 44) diffusers. The rate of increase in cross-sectional area of the optimized diffuser is significantly higher than the baseline diffuser. Figure 14 displays the surface streamlines (note change in orientation of the axes) for the optimized diffuser. The boundary-layer separation is evident in the two nodal points of separation N_1 and N_2, which correspond to the formation of the counter-rotating vortex pair evident in the twin regions of low pressure at the midpoint in Fig. 10. Additionally, the optimized diffuser incorporates a third physical factor that is absent in the baseline diffuser, namely, the contraction of the cross-sectional area downstream of the midpoint (Fig. 13). This creates a favorable streamwise pressure gradient which tends to thin the boundary layer [37].

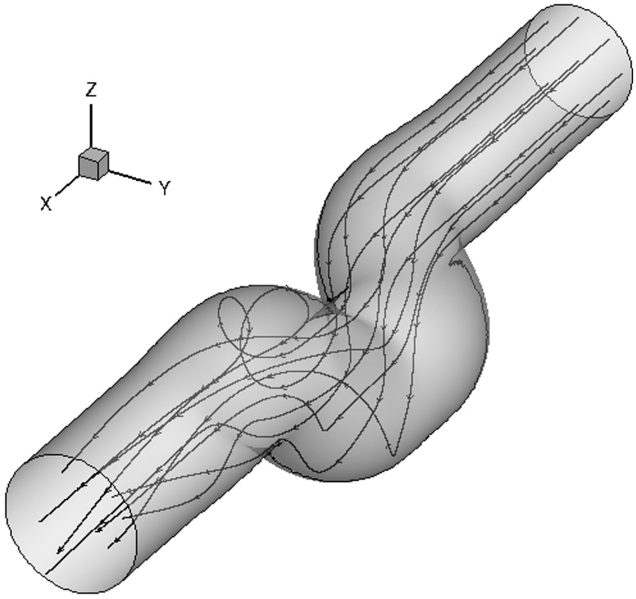

Fig. 12 Streamlines: optimized diffuser.

We therefore posit the following explanation for the reduction in distortion due to the overexpansion:

> The overexpansion at the midpoint enhances boundary-layer separation leading to greater mixing of the flow which combined with the favorable pressure gradient induced by the subsequent contraction results in a reduction in distortion at the outlet.

D. Design Principle

The results of the design optimization suggest the following simple design principle for reducing distortion in a serpentine subsonic diffuser:

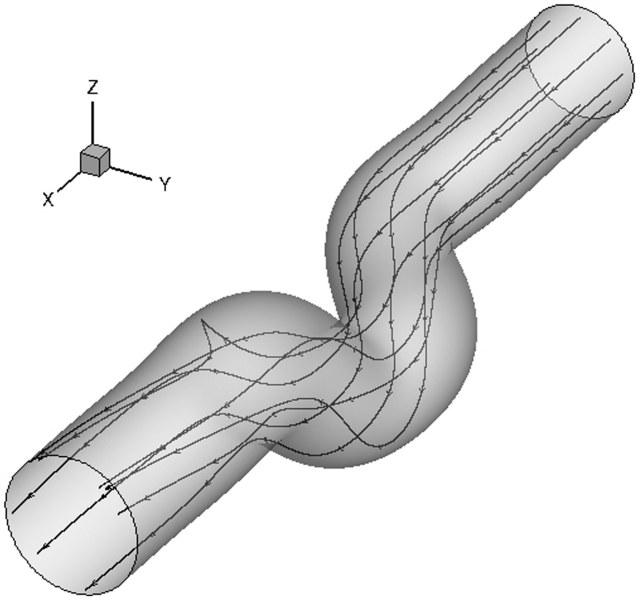

Fig. 11 Streamlines: baseline diffuser.

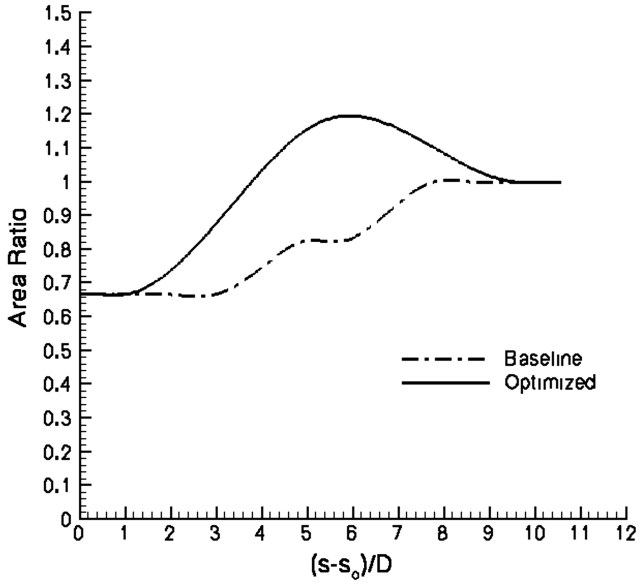

Fig. 13 Area ratio vs distance.

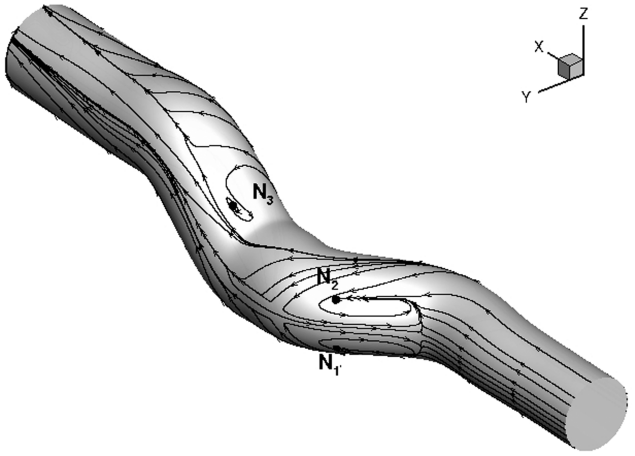

Fig. 14 Surface streamlines: optimized diffuser.

The flow in the approximate midpoint of the bends should be *overexpanded*, i.e., the cross-sectional area should be *greater* than the outlet cross-sectional area. The shape of the maximum cross-sectional area can remain approximately circular.

The smooth lofting of the cross-sectional shape of the diffuser from the circular inlet through the overexpanded section and thereafter to the circular outlet is readily performed by modern CAD software.

This simple design principle is evidently new. It does not explicitly appear in any previous automated computational design for subsonic diffusers. Lefantzi and Knight [31] used a "bump" in the bend of a S-shaped diffuser which results in a cross-sectional area at this location that exceeds the outlet cross-sectional area; however, the above simple design principle was not indicated in their paper. Nevertheless, their result is consistent with the above principle. Saha et al. [33] examined the effect of the inlet cross-sectional shape in a transitional S-duct, i.e., transition from noncircular (e.g., elliptic, semicircular, oval, rectangular, or square) inlet to a circular outlet; however, in each instance the cross-sectional area of the inlet increased monotonically from inlet to outlet. In the optimal design of Lee and Kim [23], the outlet cross-sectional area is greater than the cross-sectional area within the bend.

Certainly further research is needed to examine the validity of this simple design principle and to consider other mitigating factors including, but not limited to, the rate of overexpansion in the midsection, effects of the cross-sectional shape of the inlet, possible nonaxisymmetry of the inlet flow associated with angle of attack or sideslip, and other factors. Nevertheless, the overall simplicity of the design principle and its ease of implementation with modern CAD software warrant consideration of its use in engineering design.

V. Conclusions

A simple design principle for reducing distortion at the outlet of a serpentine subsonic diffuser is proposed. The principle states that the flow shall be overexpanded in the vicinity of the midpoint of the bend, i.e., the cross-sectional area exceed the outlet cross-sectional area. Implementation of this concept with modern CAD software is straightforward because CAD software is capable of lofting cross-sectional shapes between specified locations along a defined curved centerline.

The design principle is demonstrated for a doubly offset serpentine subsonic diffuser. An automated design optimization is performed using FLUENT software embedded in the modeFRONTIER optimization environment. The computed distortion coefficient was reduced by 56% while maintaining a high pressure recovery. Experiments indicate a 50% reduction in distortion coefficient, although the absolute values of the computed and experimental distortion coefficients differ.

Acknowledgments

The research is supported by the Agency for Defense Development, Republic of Korea, under contract U6189EF to Rutgers University, and by the U.S. Air Force Academy.

References

[1] Mattingly, J., Heiser, W., and Pratt, D., *Aircraft Engine Design*, 2nd ed., AIAA Education Series, American Institute of Aeronautics and Astronautics, Reston, VA, 2002.

[2] Kitchen, R., and Sedlock, D., "Subsonic Diffuser Development for Advanced Tactical Aircraft," *AIAA/SAE/ASME 19th Joint Propulsion Conference*, AIAA Paper No. 83-1168, June 1983.

[3] Seddon, J., and Goldsmith, E., *Intake Aerodynamics*, American Institute of Aeronautics and Astronautics, Reston, VA, 1985.

[4] Williams, D., and Surber, L., "Intake/Engine Compatability," *Practical Intake Aerodynamic Design*, edited by E. Goldsmith, and J. Seddon, American Institute of Aeronautics and Astronautics, Reston, VA, 1993, pp. 21–71.

[5] Faroukhi, S., *Aircraft Propulsion*, John Wiley & Sons, Inc., Hoboken, NJ, 2009.

[6] Bowditch, D., and Coltrin, R., "A Survey of Inlet/Engine Distortion Compatibility," NASA TM 83421, 1983.

[7] "Gas Turbine Engine Inlet Flow Distortion Guidelines," Society of Automotive Engineers International, Revision B, Warrendale, PA, 2002.

[8] Weske, J. R., "Pressure Loss in Ducts with Compound Elbows," NACA Wartime Rept. W-39, National Advisory Committee for Aeronautics, 1943.

[9] Henry, J., "Design of Power Plant Installations: Pressure Loss Characteristics of Duct Components," NACA, ARR No. L4F26, June 1944.

[10] Guo, R., and Seddon, J., "An Investigation of Swirl in an S-Duct," *The Aeronautical Quarterly*, Vol. 33, May 1982, pp. 25–58.

[11] Guo, R., and Seddon, J., "The Swirl in an S-Duct of Typical Air Intake Proportions," *The Aeronautical Quarterly*, Vol. 34, May 1983, pp. 99–128.

[12] Guo, R., and Seddon, J., "Swirl Characteristics of an S-Shaped Air Intake with Both Horizontal and Vertical Offsets," *The Aeronautical Quarterly*, Vol. 34, May 1983, pp. 130–146.

[13] Goldsmith, E., and Seddon, J., *Practical Intake Aerodynamic Design*, Blackwell Scientific Publications, Boston, 1993.

[14] Harloff, G., Reichert, B., and Wellborn, S., "Navier–Stokes Analysis and Experimental Data Comparison of Compressible Flow in a Diffusing S-Duct," AIAA Paper No. 92-2699, 1992.

[15] Jones, W., and Launder, B., "The Prediction of Laminarization with a Two-Equation Model of Turbulence," *International Journal of Heat and Mass Transfer*, Vol. 15, No. 2, 1972, pp. 301–314. doi:10.1016/0017-9310(72)90076-2

[16] Speziale, C., Ridha, A., and Anderson, E., "A Critical Evaluation of Two-Equation Models for Near Wall Turbulence," ICASE Tech. Rept. 90-46, Hampton, VA, June 1990.

[17] Abrahamsen, P., Reif, B., Saetran, L., and Fossdal, J., "Air Intake Studies: Experimental Measurements and Computational Modeling," *NATO Research and Technology Organization Meeting Proceedings 5*, NATO, Neuilly-sur-Seine, France, 1998, pp. 1–7.

[18] Chien, K., "Predictions of Channel and Boundary Layer Flows with a Low Reynolds Number Turbulence Model," *AIAA Journal*, Vol. 20, No. 1, 1982, pp. 33–38. doi:10.2514/3.51043

[19] Zhang, W., Knight, D., and Smith, D., "Automated Design of a Subsonic Diffuser," *Journal of Propulsion and Power*, Vol. 16, No. 6, 2000, pp. 1132–1140. doi:10.2514/2.5688

[20] Wellborn, S. R., Reichert, B. A., and Okiishi, T. H., "Experimental Investigation of the Flow in a Diffusing S-Duct," AIAA Paper 92-3622, 1992.

[21] Baldwin, B., and Lomax, H., "Thin Layer Approximation and Algebraic Model for Separated Turbulent Flows," AIAA Paper No. 78-257, Jan. 1978.

[22] Smith, C. F., Bruns, J. E., Harloff, G. J., and DeBonis, J. R., "Three-Dimensional Compressible Turbulent Computations for a Diffusing S-duct," NASA CR 4392, 1991.

[23] Lee, B. J., and Kim, C., "Automated Design Methodology of Turbulent Internal Flow Using Discrete Adjoint Formulation," *Aerospace Science and Technology*, Vol. 11, Nos. 2–3, 2007, pp. 163–173. doi:10.1016/j.ast.2006.12.001

[24] Kolmogorov, A. N., "*Equations of Turbulent Motion of an Incompressible Fluid*," Izvestia Academy of Sciences, Vol. 6, Nos. 1–2, 1942, pp. 56–58.
[25] Saffman, P. G., "A Model for Inhomogeneous Turbulent Flow," *Proceedings of the Royal Society of London*, Vol. A317, 1970, pp. 417–433.
[26] Kaldschmidt, G., Syltebo, B., and Ting, C., "A 727 Airplane Center Duct Inlet Low Speed Performance Confirmation Model Test for Refanned JT8D Engines, Phase II," NASA CR-134534, November 1973.
[27] Anderson, B. H., "Vortex-Generator Installation Studies on Steady-State and Dynamic Distortion," *Journal of Aircraft*, Vol. 35, No. 4, 1998, pp. 513–520.
doi:10.2514/2.2340
[28] Jirásek, A., "Design of Vortex Generator Flow Control in Inlets," *Journal of Aircraft*, Vol. 43, No. 6, Nov.–Dec. 2006, pp. 1886–1892.
doi:10.2514/1.21364
[29] Mayer, D., Anderson, B., and Johnson, T., "3D Subsonic Diffuser Design and Analysis," *34th AIAA/ASME/ASEE Joint Propulsion Conference*, AIAA Paper No. 98-3418, July 1998.
[30] Cholaseuk, D., Srinivasan, V., and Modi, V., "Shape Optimization for Fluid Flow Problems Using Bezier Curves and Designed Numerical Experiments," *Proceedings of the 1999 ASME Design Engineering Technical Conferences*, American Society of Mechanical Engineers, New York, Sept. 1999.
[31] Lefantzi, S., and Knight, D., "Automated Design of a Three-Dimensional S-Shaped Subsonic Diffuser," *Journal of Propulsion and Power*, Vol. 18, No. 4, 2002, pp. 913–921.
doi:10.2514/2.6017
[32] Lim, S., and Choi, H., "Optimal Shape Design of a Two-Dimensional Asymmetric Diffuser in Turbulent Flow," *AIAA Journal*, Vol. 42, No. 6, June 2004, pp. 1154–1169.
doi:10.2514/1.3234
[33] Saha, K., Singh, N., and Seshadri, V., "Computational Analysis of Flow Through Transition S-Diffusers: Effect of Inlet Shape," *Journal of Aircraft*, Vol. 44, No. 1, 2007, pp. 187–193.
doi:10.2514/1.22828
[34] Wilcox, D., *Turbulence Modeling for CFD*, DCW Industries, Inc., La Cañada, CA, 1994.
[35] Stephens, D., and Wyst, E. V., "Comparing Computational to Experimental Flow Quality of Subsonic Serpentine Inlets," U.S. Air Force Academy Department of Aeronautics, Final Rept. AE 471, 2008.
[36] Cox, J., Paul, M., Cummings, R., and Byerley, A., "Experimental Validation of Computational Design Optimizer Method for Two-Axis Offset Serpentine Inlet," U.S. Air Force Academy Department of Aeronautics, Final Rept. AE471, 2009.
[37] Greitzer, E., Tan, C., and Graf, M., *Internal Flow Concepts and Applications*, Camridge Univ. Press, Cambridge, England, U.K., 2004.

F. Liu
Associate Editor